NUMERICAL INVESTIGATIONS OF HYDRODYNAMIC CHARACTERISTICS OF A MARINE-FOULED SUBMERGED FLOATING TUNNEL

Pengxu Zou, Delft University of Technology, p.zou@tudelft.nl
Niels Ruiter, Delft University of Technology, nielsruiter@hotmail.com
Jeremy Bricker, University of Michigan, jeremydb@umich.edu
Wim S.J. Uijttewaal, Delft University of Technology,W.S.J.Uijttewaal@tudelft.nl

INTRODUCTION

Marine biofouling is a major concern in the operational performance of submerged floating tunnels (SFTs). Within years after construction, marine growth increases the effective dimension and mass of the SFT and hence, can substantially affect the hydrodynamic forces and alter the buoyancy-weight ratio (BWR). Therefore, roughness height is one of the most crucial factors influencing the hydrodynamic performance of the SFT. In addition, Schultz (Schultz, 2007) found that fouling greatly affects ship resistance and power requirement. However, existing studies of drag and lift coefficients contradict to each other due to different experimental set-ups, Reynolds number ranges, and roughness length scales (Zeinoddini et al., 2016). Such conclusions cannot be directly adaptable to the SFTs due to its unique structural properties and environmental conditions. Therefore, we investigated the effects of marine fouling and flow behavior around the SFT with varying roughness properties at different Reynolds numbers. Furthermore, the cross-section geometry of an SFT has a significant effect on flow behavior. However, most previous marine fouling research is mainly based on simpler sections such as circular shapes (Henry et al., 2016). In this study, resistance characteristics for marine fouling on an SFT with two cross-section shapes (i.e., circular and parametric shapes) are investigated and compared (P. Zou et al., 2020).

METHODOLOGY

In this study, the influence of increased surface roughness as caused by marine fouling on an SFT is investigated using Computational Fluid Dynamics (CFD). The roughness created by hard fouling is one of the main drivers of hydrodynamic changes (Marty et al., 2021). We choose a schematized pyramid-shaped roughness to reduce the uncertainties with complex biological processes involved, and a staggered pattern of roughness elements is designed to avoid sheltering effects. The influence of SFT cross-section shape, roughness height, and fouling coverage ratio on the hydrodynamic forces of an SFT are comparatively analyzed under various current conditions. Unsteady Reynolds Averaged Navier-Stokes (URANS) based transitional turbulence models are applied for flow characteristics predictions such as flow separation, vortex shedding, and wake parameters (Zou et al., 2021). The transient solver *PimpleFoam,* supplied with OpenFOAM, for incompressible, turbulent flow is applied for current conditions. The merged PISO-SIMPLE (PIMPLE) algorithm is applied to solve the pressure-velocity coupling and correction. The *Transition SST* (Shear Stress Transport) model is applied for the transition onset prediction (Langtry & Menter, 2009). Besides the two-equation model including the *k* and *ω* equations of the *k-ω* SST turbulence model, the additional transport equations of the *Transition SST* model are shown in Eq.(1)

$$\begin{cases} \frac{\partial}{\partial t}(\rho\gamma)+\frac{\partial}{\partial x_j}(\rho\gamma U_j)=\frac{\partial}{\partial x_j}[(\mu+\frac{\mu_t}{\sigma_\gamma})\frac{\partial\gamma}{\partial x_j}]+P_{\gamma1}-E_{\gamma1}+P_{\gamma2}-E_{\gamma2} \\ \frac{\partial}{\partial t}(\rho \tilde{Re}_{\theta t})+\frac{\partial}{\partial x_j}(\rho \tilde{Re}_{\theta t} U_j)=\frac{\partial}{\partial x_j}[\sigma_{\theta t}(\mu+\mu_t)\frac{\partial \tilde{Re}_{\theta t}}{\partial x_j}]+P_{\theta t} \end{cases} \quad (1)$$

where σ_γ=1.0, and $\sigma_{\theta t}$=2.0. μ is viscosity. μ_t is eddy viscosity. p_∞ is reference pressure. $P_{\gamma 1}$ and $E_{\gamma 1}$ are transition sources. $P_{\gamma 2}$ and $E_{\gamma 2}$ are destruction and relaminarization sources. $P_{\theta t}$ is production source term. γ is intermittency. $\widetilde{Re_{\theta t}}$ is transition momentum thickness Reynolds number; ρ is fluid density. U is flow velocity.

NUMERICAL VALIDATION AND SET-UP

The numerical results for current interactions with rough SFTs are validated against small-scale laboratory experiments performed at Delft University of Technology (TU Delft). In order to reproduce the experiments, validate the numerical results, and resolve the 3-dimensional roughness elements, 3-dimensional numerical models with different roughness parameters are established. The computational domain is 8 m in length and 0.7 m in height (equivalent to the water depth in the experiments). The center of the SFT is located 2 m from the inlet, with an internal blockage length (smooth SFT) of 16 cm. Due to the uniformly distributed roughness elements along the SFT span, the thickness of the numerical domain is determined by the length of the repetitive roughness pattern and truncated in the symmetry side planes. The typical grid layout is shown in Fig.1. The freestream conditions for velocity and pressure are employed at both the inlet and outlet boundary. The turbulence intensity at the inlet is 6%, which is consistent with the experiments. A simplified no-slip wall condition is applied on the SFT cross-section surface and at the bottom boundary. A free-slip wall is used at the upper boundary. A high-quality unstructured mesh is generated around the SFT cross-section surface. The first grid layer cell length normal to the SFT surface is determined by making the wall y^+ around 1. The total number of cells is around 2 million.

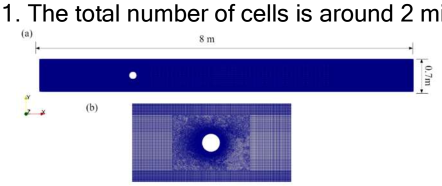

Figure 1 – (a) Computational domain of the numerical

model; (b) Mesh detail near the SFT.

In order to investigate the effects of marine fouling on the hydrodynamic forces of the SFT, a sensitivity analysis of roughness parameters and cross-section shape is carried out. The roughness parameters are shown in Table 1 and Fig.2.

Table 1 Model parameters

Model conditions	
Current speed U (m/s)	0.05, 0.1, 0.2, 0.3
SFT cross-section shape	circular, parametric
Roughness parameters	
Roughness height k (cm)	0.5, 1.0, 1.5
Roughness coverage ratio (%)	25, 50, 100

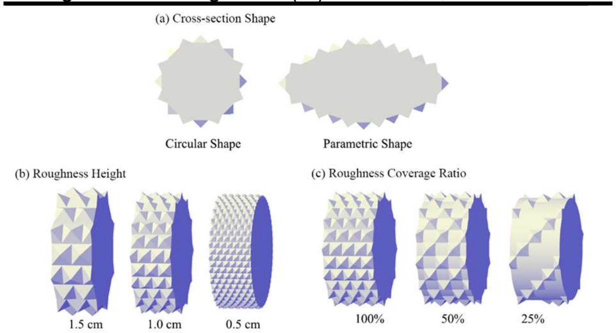

Figure 2 - SFT shapes and roughness parameters.

The equivalent diameter (D_e) of the rough SFT is determined by an equal blockage area. The numerical results of the mean drag coefficient ($C_d=F_{x,m}/(0.5\times D_e \times\rho\times U^2$; $F_{x,m}$ is mean drag force) for the SFT with a roughness height of 1.5 cm for circular and parametric shapes are plotted against R_e and compared with experimental data in Fig.3. The maximum relative error is 9.1% at R_e = 1.6×10^4 with the parametric shape, due to experimental uncertainties and numerical assumptions. Despite the small deviations, numerical results and the experimental data are considered a reasonable agreement, implying the validity of the numerical results. Since the lift forces are measured on the entire cylinder in the experiments with the low spanwise correlation effects (vortex shedding is not synchronised over the length of the SFT), it is not possible to compare the lift coefficients to the experiments.

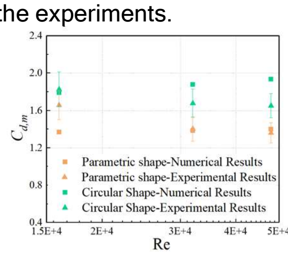

Figure 3 -Hydrodynamic force coefficients validation

RESULTS ANALYSIS

Effect of SFT cross-section shape

Mean drag coefficient and Root Mean Square (RMS) fluctuating lift coefficient ($C_{l,rms}=F_{y,rms}/(0.5\times D_e \times\rho\times U^2$; $F_{y,rms}$ is RMS fluctuating lift force) with a fixed roughness height of 1.5 cm and coverage ratio of 100 % for circular and parametric shapes are plotted against R_e in Fig.4. It shows that with an equal blockage height, the parametric shape has a much lower $C_{d,m}$ and $C_{l,rms}$ compared to the circular shape. In addition, the clearance for transportation is much larger, which increases space utilization (Fig.2(a)).

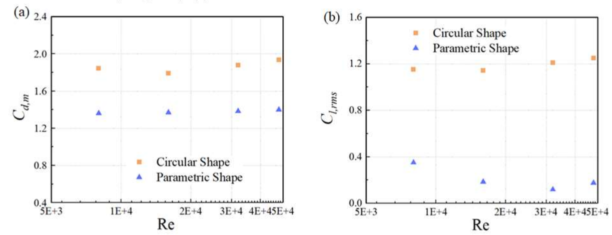

Figure 4 -Hydrodynamic force coefficients for different cross-section shapes. (a) $C_{d,m}$ vs R_e;(b) $C_{l,rms}$ vs R_e.

The schematic of the mean velocity contour behind the SFT with two cross-section shapes is shown in Fig.5. It can be observed that the formation length of the recirculation region behind the parametric shape is longer due to its more streamlined shape, but the wake width of the parametric shape is shorter than the circular shape (flow separation point moves more downstream), leading to the drag and fluctuating lift reduction.

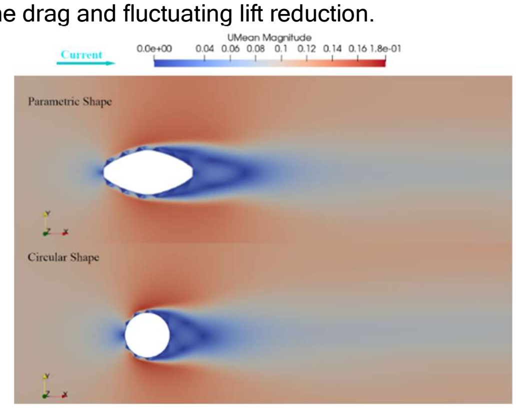

Figure 5 - Mean velocity contours for rough SFTs with different cross-section shapes, R_e = 1.6×10^4, Unit: m/s.

Effect of roughness height

Fig.6 shows $C_{d,m}$ and $C_{l,rms}$ against R_e for different roughness heights with the circular shape and an equal roughness coverage ratio of 100%. It shows that $C_{d,m}$ and $C_{l,rms}$ increases with increasing roughness height.

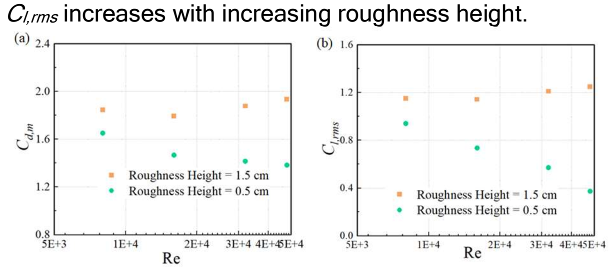

Figure 6 -Hydrodynamic force coefficients for different roughness heights. (a) $C_{d,m}$ vs R_e;(b) $C_{l,rms}$ vs R_e.

The mechanism underlying the variations of $C_{d,m}$ and $C_{l,rms}$ with the roughness height can be interpreted from the mean velocity contour behind the SFTs in Fig.7. For the case k = 1.5 cm, due to the exaggerated roughness height and 3-dimensional properties of the roughness elements, the cross-stream spacing of the primary eddies and recirculation length increase with increasing roughness height due to the large blockage area, and hence, enhances the drag.

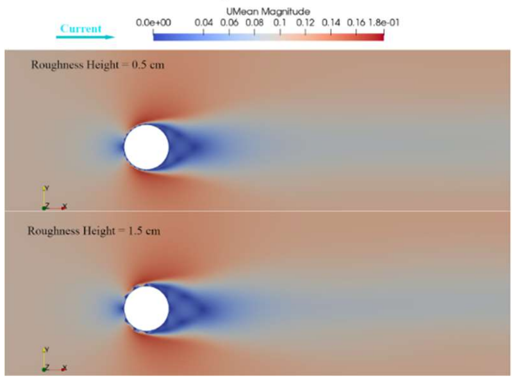

Figure 7 – Mean velocity contours of rough SFTs with different roughness heights, $R_e = 1.6\times10^4$, Unit: m/s.

Effect of roughness coverage ratio

Fig.8 shows $C_{d,m}$ and $C_{l,rms}$ variations against R_e for different roughness coverage ratios with the circular shape and an equal roughness height of 1.0 cm. It can be seen that $C_{d,m}$ and $C_{l,rms}$ increase with increasing roughness coverage ratio. However, the rate of increase slows down.

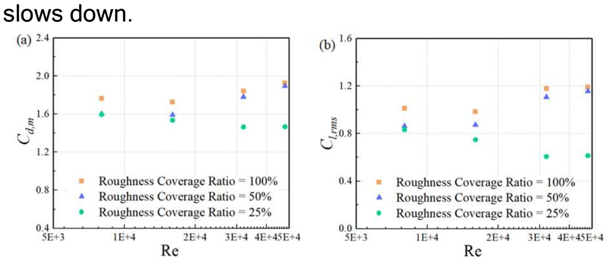

Figure 8 –Hydrodynamic force coefficients for different roughness coverage ratios. (a) $C_{d,m}$ vs R_e; (b) $C_{l,rms}$ vs R_e.

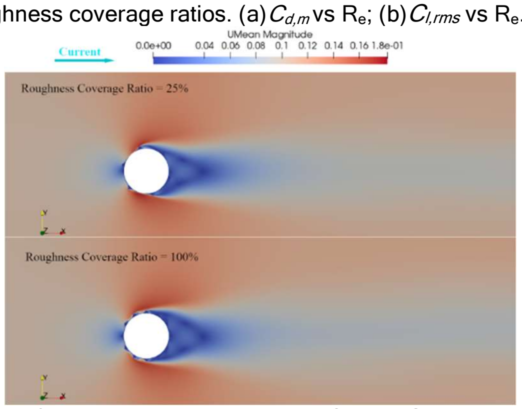

Figure 9 – Mean velocity contours of rough SFTs with different roughness coverage ratios, $R_e = 1.6\times10^4$, Unit: m/s.

Fig.9 shows the mean velocity contour behind the SFT with two roughness coverage ratios. As can be seen, for a coverage ratio of 25%, the wake width is narrower, compared to the 50% case. Additionally, the flow separation point for the coverage ratio of the 25% case occurs further downstream than that of the 50% case. Both mechanisms contribute to the reduction of drag and fluctuating lift forces for the coverage ratio of 25% case.

CONCLUSIONS

This paper presents numerical findings of marine fouling effects on the hydrodynamic forces and flow characteristics of an SFT over the range $8\times10^3 \leq R_e \leq 4.8\times10^4$. The results show the SFT cross-section with the parametric shape is preferable for its force mitigating effects. Roughness height is a crucial factor for hydrodynamic forces, affecting the flow separation and blockage area of the SFT. The hydrodynamic forces increase with increasing coverage ratio but the trend slows down. The current study presents marine fouling effects on the SFTs in detail for the first time. The evaluated findings of hydrodynamic force in relation to roughness function variables can provide references for dynamic response and reliability analyses and the design optimization of SFTs.

REFERENCES

Henry, P. Y., Nedrebø, E. L., & Myrhaug, D. (2016). Visualisation of the effect of different types of marine growth on cylinders' wake structure in low Re steady flows. *Ocean Engineering*, *115*. https://doi.org/10.1016/j.oceaneng.2016.02.023

Langtry, R. B., & Menter, F. R. (2009). Correlation-based transition modeling for unstructured parallelized computational fluid dynamics codes. *AIAA Journal*. https://doi.org/10.2514/1.42362

Marty, A., Berhault, C., Damblans, G., Facq, J. V., Gaurier, B., Germain, G., Soulard, T., & Schoefs, F. (2021). Experimental study of hard marine growth effect on the hydrodynamical behaviour of a submarine cable. *Applied Ocean Research*, *114*. https://doi.org/10.1016/j.apor.2021.102810

Schultz, M. P. (2007). Effects of coating roughness and biofouling on ship resistance and powering. *Biofouling*, *23*(5). https://doi.org/10.1080/08927010701461974

Zeinoddini, M., Bakhtiari, A., Ehteshami, M., & Seif, M. S. (2016). Towards an understanding of the marine fouling effects on VIV of circular cylinders: Response of cylinders with regular pyramidal roughness. *Applied Ocean Research*, *59*. https://doi.org/10.1016/j.apor.2016.05.013

Zou, P., Bricker, J., & Uijttewaal, W. (2020). Optimization of submerged floating tunnel cross section based on parametric Bézier curves and hybrid backpropagation - genetic algorithm. *Marine Structures*, *74*. https://doi.org/10.1016/j.marstruc.2020.102807

Zou, Pengxu, Bricker, J. D., & Uijttewaal, W. (2021). Submerged floating tunnel cross-section analysis using a transition turbulence model. *Journal of Hydraulic Research*. https://doi.org/10.1080/00221686.2021.1944921